

Numerical studies of thermal convection with temperature- and pressure-dependent viscosity at extreme viscosity contrasts

Cite as: Phys. Fluids **27**, 076603 (2015); <https://doi.org/10.1063/1.4923061>

Submitted: 01 April 2015 . Accepted: 16 June 2015 . Published Online: 07 July 2015

Tania S. Khaleque, A. C. Fowler, P. D. Howell , and M. Vynnycky 



View Online



Export Citation



CrossMark

ARTICLES YOU MAY BE INTERESTED IN

[Numerical investigation of 2D convection with extremely large viscosity variations](#)

Physics of Fluids **7**, 2154 (1995); <https://doi.org/10.1063/1.868465>

[Scaling of temperature- and stress-dependent viscosity convection](#)

Physics of Fluids **7**, 266 (1995); <https://doi.org/10.1063/1.868624>

[On the Rayleigh number dependence of convection with a strongly temperature-dependent viscosity](#)

Physics of Fluids **10**, 351 (1998); <https://doi.org/10.1063/1.869527>



Highlights of the best new research
in the physical sciences

[LEARN MORE!](#)





Numerical studies of thermal convection with temperature- and pressure-dependent viscosity at extreme viscosity contrasts

Tania S. Khaleque,^{1,a)} A. C. Fowler,^{1,2} P. D. Howell,¹ and M. Vynnycky³

¹OCIAM, Mathematical Institute, University of Oxford, Oxford, United Kingdom

²MACSI, University of Limerick, Limerick, Ireland

³KTH Royal Institute of Technology, Stockholm, Sweden

(Received 1 April 2015; accepted 16 June 2015; published online 7 July 2015)

Motivated by convection of planetary mantles, we consider a mathematical model for Rayleigh-Bénard convection in a basally heated layer of a fluid whose viscosity depends strongly on temperature and pressure, defined in an Arrhenius form. The model is solved numerically for extremely large viscosity variations across a unit aspect ratio cell, and steady solutions for temperature, isotherms, and streamlines are obtained. To improve the efficiency of numerical computation, we introduce a modified viscosity law with a low temperature cutoff. We demonstrate that this simplification results in markedly improved numerical convergence without compromising accuracy. Continued numerical experiments suggest that narrow cells are preferred at extreme viscosity contrasts, and this conclusion is supported by a linear stability analysis. © 2015 AIP Publishing LLC. [<http://dx.doi.org/10.1063/1.4923061>]

I. INTRODUCTION

Steady Rayleigh-Bénard convection of an infinite Prandtl number Boussinesq fluid heated from below in a rectangular box with stress-free boundaries has become a benchmark problem in computational geophysics as a paradigm for convection in the Earth's mantle. Assessments of the mantle viscosity beneath the relatively rigid lithosphere indicate a relatively uniform viscosity of about 10^{21} Pa s,^{1,2} and subsequent studies have not essentially altered that conclusion (e.g., Paulson *et al.*³). Early studies of mantle convection therefore assumed a constant viscosity, and both numerical and analytic studies appeared to give a satisfactory explanation for plate tectonic observations on the Earth, for example, the lithosphere plates are identified with thermal boundary layers of the convection cells.^{4–8}

In reality, the effective viscosity of the mantle is a strong function of temperature, pressure, and stress. The temperature and stress dependences are well documented experimentally; the pressure dependence is less constrained, but reasonable estimates for all these dependences are available.^{9,10} The typical values of the parameters relevant to the Earth are given later in Table I. These values suggest that the viscosity contrast across the mantle is of order 10^{50} or more. The parameter values corresponding to other terrestrial planets also indicate that the approximate viscosity variation is of orders 10^{20} (Venus) and 10^{50} or more (Mars).^{11–13} Boundary layer analysis and numerical experiments show that temperature dependence of the viscosity leads to an extremely viscous, effectively rigid, cold upper thermal boundary layer, which represents the lithosphere. The resulting “stagnant lid” convection is unlike that seen in the Earth,¹⁴ and the active style of tectonics on Earth is generally thought to be a consequence of weakening at high stress, due either to stress-dependent viscosity or plastic yielding.^{15–21} Temperature dependence of the viscosity thus does not fully capture the qualitative features observed in mantle convection in the Earth.

The effect in convection of viscosity depending strongly on both temperature and pressure does not appear to have attracted the attention it deserves, either analytically or computationally.

^{a)}E-mail: khaleque@maths.ox.ac.uk

TABLE I. Typical parameter values for mantle convection.

Symbol	Parameter	Value	Units
d	Mantle depth	3×10^6	m
α	Thermal expansion coefficient	2×10^{-5}	K^{-1}
ρ_0	Reference density	4×10^3	kg m^{-3}
κ	Thermal diffusivity	1×10^{-6}	$\text{m}^2 \text{s}^{-1}$
g	Gravitational acceleration	10	m s^{-2}
T_s	Surface temperature	300	K
T_b	Basal temperature	3000	K
E	Activation energy	300–525	kJ mol^{-1}
V	Activation volume	6×10^{-6}	$\text{m}^3 \text{mol}^{-1}$
R	Universal gas constant	8.31	$\text{J mol}^{-1} \text{K}^{-1}$
A	Viscous rate constant	10^5	$\text{MPa}^{-1} \text{s}^{-1}$
Ra	Rayleigh number	10^7 – 10^9	
ε	Viscous temperature number	0.042–0.083	
μ	Viscous pressure number	1.2–2.4	
\overline{B}	Boussinesq number	0.06	
θ_0	Dimensionless surface temperature	0.1	

This is undoubtedly due to the fact that, from both points of view, it is a very difficult problem. Confronted with the goal of computing convective solutions with viscosity varying by factors in the region of 10^{50} , the challenge is to approach such extreme contrasts sufficiently that the correct limiting asymptotic structure is reached. Very early attempts foundered on the computational difficulty which extreme viscosity contrasts caused. In the 1980s, Christensen and his co-workers^{22–25} were able to compute models with viscosity contrasts up to about 10^6 . Solomatov and his co-workers were later able to extend these results up to viscosity contrasts around 10^{15} .^{26–29} The influence of temperature and depth-dependent viscosity on convection has also been explored in two-dimensional numerical experiments by Fleitout and Yuen,³⁰ Doin *et al.*,³¹ and Stemmer *et al.*³² in different forms.

In this paper, we present computational results for steady convection when the viscosity is an Arrhenius function that depends extremely sensitively on both temperature and pressure. We start in Sec. II by stating and normalising the governing equations and boundary conditions. In Sec. III, we describe our computational approach and validate our method through comparison with benchmark values from the literature. We then present preliminary numerical results which demonstrate that the inclusion of pressure dependence profoundly changes the flow structure compared with purely temperature-dependent results. Surprisingly, large viscosity variations, by a factor of up to 10^{30} , are required to observe the new flow regime, which perhaps explains why it has not previously been observed. To facilitate the study of such extreme cases, in Sec. IV, we propose a cutoff viscosity relation that alleviates the computational stiffness while retaining the sensitivity of the viscosity to changes in temperature and pressure. This approach allows us to consider even higher viscosity contrasts, and we show that the resulting flow breaks into increasingly narrow convection cells. This observation is supported by a linear stability analysis. A discussion follows in Sec. V, and finally, we draw our conclusions in Sec. VI.

II. GOVERNING EQUATIONS

A. Model equations and boundary conditions

We consider classical Rayleigh-Bénard convection in a two-dimensional rectangular cell of depth d and width ad , with a fixed temperature difference between the horizontal boundaries. This convective cell is assumed to be a part of a periodic structure in an infinite horizontal layer. We adopt Cartesian coordinates (x, z) with the x -axis horizontal and the z -axis pointing vertically

upwards. The governing equations ensure the conservation of mass, momentum, and energy, and are completed by a suitable thermodynamic equation of state. We make the Boussinesq approximation and neglect the inertia terms in the Navier–Stokes equations (taking the limit of infinite Prandtl number), so that the governing equations read

$$\begin{aligned}
 \frac{\partial u}{\partial x} + \frac{\partial w}{\partial z} &= 0, \\
 \frac{\partial p}{\partial x} &= \frac{\partial \tau_1}{\partial x} + \frac{\partial \tau_3}{\partial z}, \\
 \frac{\partial p}{\partial z} &= \frac{\partial \tau_3}{\partial x} - \frac{\partial \tau_1}{\partial z} - \rho g, \\
 \tau_1 &= 2\eta \frac{\partial u}{\partial x}, \\
 \tau_3 &= \eta \left(\frac{\partial u}{\partial z} + \frac{\partial w}{\partial x} \right), \\
 \rho &= \rho_0 [1 - \alpha (T - T_b)], \\
 \frac{\partial T}{\partial t} + \mathbf{u} \cdot \nabla T &= \kappa \nabla^2 T,
 \end{aligned} \tag{2.1}$$

where u and w are velocity components in the x - and z -directions, t is the time, p is the pressure, τ_1 and τ_3 are the longitudinal and shear components of the deviatoric stress tensor, respectively, ρ is the density, T is the absolute temperature, and η is the viscosity. The parameters in the model are the gravitational acceleration g , thermal expansion coefficient α , basal temperature T_b , basal density ρ_0 , and thermal diffusivity κ . We use the following constitutive relation for the viscosity:

$$\eta = \frac{1}{2A(\tau_1^2 + \tau_3^2)^{(n-1)/2}} \exp \left\{ \frac{E + pV}{RT} \right\}, \tag{2.2}$$

where A is the rate factor, n is the flow index, E is the activation energy, V is the activation volume, and R is the universal gas constant.

We impose free-slip boundary conditions on all boundaries and thermal insulation on the vertical sides. The base and top of the cell are assumed to be at specified temperatures T_b and T_s , respectively, so the boundary conditions are

$$\begin{aligned}
 w &= 0, \quad \tau_3 = 0, \quad T = T_b & \text{on } z = 0, \\
 w &= 0, \quad \tau_3 = 0, \quad T = T_s & \text{on } z = d, \\
 u &= 0, \quad \tau_3 = 0, \quad \frac{\partial T}{\partial x} = 0 & \text{on } x = 0, ad,
 \end{aligned} \tag{2.3}$$

where d is the depth of the convection cell.

In addition to the assumptions noted above, we have also neglected internal heating and isothermal compressibility; radiogenic heating may be significant but is not necessary, since basal heating from the Earth's core suffices to induce vigorous convection.³³ We also treat the thermal diffusivity as constant. It should be noted also that the assumption of a Cartesian geometry is not appropriate for the mantle, but this is unlikely to make a substantial difference to the results.³³ Throughout this paper, we will consider only Newtonian rheology, and we therefore set $n = 1$ henceforth.

B. Non-dimensionalisation

Following Fowler³³ and Jarvis and Peltier,⁸ we non-dimensionalise as follows:

$$\begin{aligned}
 (x, z) &= d(x^*, z^*), \quad T = T_b T^*, \quad u = \frac{\kappa}{d} u^*, \quad \eta = \frac{e^{(1+\mu)/\varepsilon}}{2A} \eta^* = \eta_0 \eta^*, \\
 \tau &= \frac{\eta_0 \kappa}{d^2} \tau^*, \quad \rho = \rho_0 \rho^*, \quad t = \frac{d^2}{\kappa} t^*, \quad p = \rho_0 g d (1 - z^*) + \frac{\eta_0 \kappa}{d^2} p^*.
 \end{aligned} \tag{2.4}$$

Governing equations (2.1) become, on dropping the asterisk decoration,

$$\begin{aligned}
 \frac{\partial u}{\partial x} + \frac{\partial w}{\partial z} &= 0, \\
 \frac{\partial p}{\partial x} &= \frac{\partial \tau_1}{\partial x} + \frac{\partial \tau_3}{\partial z}, \\
 \frac{\partial p}{\partial z} &= \frac{\partial \tau_3}{\partial x} - \frac{\partial \tau_1}{\partial z} - \text{Ra}(1 - T), \\
 \tau_1 &= 2\eta \frac{\partial u}{\partial x}, \\
 \tau_3 &= \eta \left(\frac{\partial u}{\partial z} + \frac{\partial w}{\partial x} \right), \\
 \frac{\partial T}{\partial t} + \mathbf{u} \cdot \nabla T &= \nabla^2 T,
 \end{aligned} \tag{2.5}$$

while the dimensionless version of constitutive relation (2.2) (with $n = 1$) reads

$$\eta = \exp \left[\frac{1 - T + \mu \{1 - z - T + \bar{B}p/\text{Ra}\}}{\varepsilon T} \right]. \tag{2.6}$$

The remaining parameters in the model are defined by

$$\text{Ra} = \frac{\alpha \rho_0 g T_b d^3}{\eta_0 \kappa}, \quad \varepsilon = \frac{RT_b}{E}, \quad \mu = \frac{\rho_0 g d V}{E}, \quad \bar{B} = \alpha T_b, \quad \theta_0 = \frac{T_s}{T_b}. \tag{2.7}$$

Typical parameter values are given in Table I. For $\text{Ra} \gg 1$, we can see that \bar{B}/Ra can be easily ignored, and viscosity relation (2.6) may therefore be simplified to

$$\eta = \exp \left[\frac{1 - T + \mu(1 - z - T)}{\varepsilon T} \right]. \tag{2.8}$$

Finally, the dimensionless versions of boundary conditions (2.3) read

$$\begin{aligned}
 w = 0, \quad \tau_3 = 0, \quad T = 1 & \quad \text{on } z = 0, \\
 w = 0, \quad \tau_3 = 0, \quad T = \theta_0 & \quad \text{on } z = 1, \\
 u = 0, \quad \tau_3 = 0, \quad \frac{\partial T}{\partial x} = 0 & \quad \text{on } x = 0, a.
 \end{aligned} \tag{2.9}$$

Our complete dimensionless model consists of governing equations (2.5), constitutive relation (2.8), and boundary conditions (2.9).

C. Viscosity contrast, Nusselt number, and root mean square (RMS) velocity

We now define three useful diagnostic quantities which will be used to characterise the numerical results found below. First, we define the viscosity contrast $\Delta\eta$ to be the ratio between the surface and basal values of the viscosity, that is,

$$\Delta\eta = \exp \left(\frac{1 - \theta_0 - \mu\theta_0}{\varepsilon\theta_0} \right). \tag{2.10}$$

Second, the Nusselt number Nu measures the ratio of the average surface heat flow from the convective solution to the heat flow due to conduction alone and is calculated by

$$\text{Nu} = -\frac{1}{a(1 - \theta_0)} \int_0^a \frac{\partial T}{\partial z}(x, 1) dx. \tag{2.11}$$

Finally, the vigour of the circulating flow is characterised by the non-dimensional RMS velocity, defined by

$$V_{\text{rms}} = \left[\int_0^1 \int_0^a (u^2 + w^2) \, dx \, dz \right]^{1/2}. \quad (2.12)$$

III. NUMERICAL INVESTIGATION

A. Computational method

We used the finite element based PDE software Comsol Multiphysics to solve numerically the dimensionless equations derived in Sec. II. Lagrangian triangular elements were used for the laminar flow and the heat equation (quadratic elements for u , w , T and linear elements for p). We used extra fine meshing for the whole domain with refinement near the boundaries (200×200) which results in a complete mesh of 17 180 elements with 115 276 degrees of freedom (N_{dof}). For all cases, the same convergence criterion was applied, namely,

$$\left(\frac{1}{N_{\text{dof}}} \sum_{i=1}^{N_{\text{dof}}} |E_i|^2 \right)^{1/2} < \epsilon, \quad (3.1)$$

where E_i is the estimated error in the current approximation to the i th component of the solution vector and $\epsilon = 10^{-6}$.

To validate our model, we compared the computed values of Nusselt number Nu and root mean square velocity V_{rms} with benchmark values from Blankenbach *et al.*³⁴ and Koglin, Jr. *et al.*³⁵ for the constant viscosity case, using $a = 1$. Their values were computed for Ra up to 10^6 and 10^7 , respectively. The comparison is shown in Table II, where we can observe that the agreement is within a very good range. In this present work, we have successfully computed the values of Nu and V_{rms} for $Ra = 10^8$ and $Ra = 10^9$, and we present these also in Table II. For the case of temperature-dependent viscosity, we compared our results with King³⁶ and likewise obtained excellent agreement with errors less than 0.05%.

B. Results

We first solve model problems (2.5), (2.8), and (2.9) in a unit aspect ratio cell ($a = 1$) using the computational method outlined above. In all the results shown in this section, we fix a large value of the Rayleigh number $Ra = 10^7$ and the dimensional surface temperature $\theta_0 = 0.1$.

In Figure 1, we demonstrate the significant effects of including pressure dependence in viscosity relation (2.8). The left-hand panels (a) and (c) show temperature profiles in the convecting cell with $\mu = 0$ so that the viscosity depends only on the temperature. In the right-hand panels (b) and (d), we show the corresponding results when pressure dependence is included, with $\mu = 1$. In each plot, the blue region indicates a cold thermal boundary layer at the top of the cell, where the fluid

TABLE II. Comparison of Nusselt number Nu and RMS velocity V_{rms} with benchmark values from Blankenbach *et al.*³⁴ and Koglin, Jr. *et al.*³⁵

Ra	Nu			V_{rms}		
	This work	Benchmark	Error (%)	This work	Benchmark	Error (%)
10^4	4.884 47	4.884 409	0.001	42.865 56	42.864 947	0.0016
10^5	10.534 31	10.534 095	0.002	193.218 59	193.214 54	0.002
10^6	21.972 99	21.972 465	0.002	834.013 19	833.989 77	0.0028
10^7	45.639 39	45.62	0.04	3 633.386 85
10^8	95.572 20	16 157.877 30
10^9	201.312 45	72 930.103 52

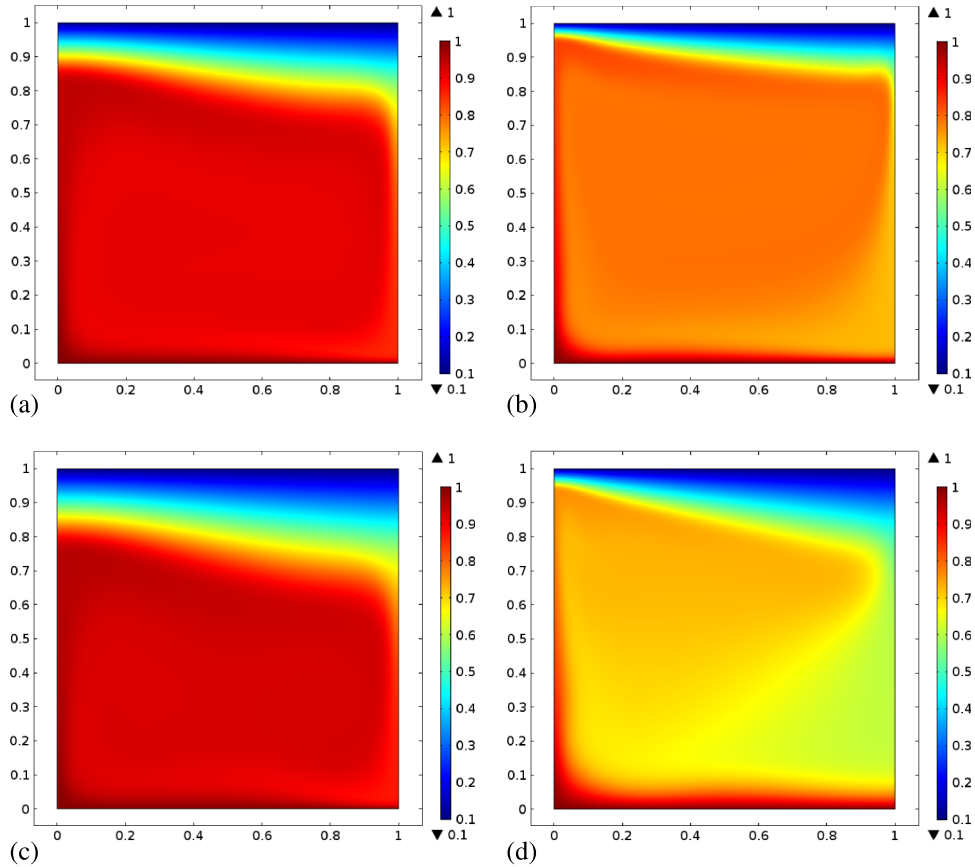


FIG. 1. Thermal distributions of a temperature-dependent viscosity convection ((a) and (c)) and a temperature- and pressure-dependent viscosity convection ((b) and (d)) at different viscosity variations for $\theta_0 = 0.1$ and $Ra = 10^7$. (a) $\varepsilon = 0.195$, $\mu = 0$, $\Delta\eta = 1.1 \times 10^{20}$; (b) $\varepsilon = 0.195$, $\mu = 1.0$, $\Delta\eta = 6.6 \times 10^{17}$; (c) $\varepsilon = 0.1303$, $\mu = 0$, $\Delta\eta = 9.9 \times 10^{29}$; and (d) $\varepsilon = 0.1303$, $\mu = 1.0$, $\Delta\eta = 4.6 \times 10^{26}$.

is extremely viscous and forms an effectively rigid lid. Both with and without pressure dependence, the thickness of the lid increases as the viscosity contrast gets larger. However, in the rest of the cell, the differences between the left and right-hand panels are striking.

When $\mu = 0$, so the viscosity depends only on temperature, the fluid is roughly isothermal outside the lid and thin thermal boundary layers on the base and sides of the cell. The presence of an isothermal core eliminates the extreme viscosity contrast in the bulk flow. However, when $\mu = 1$, it is no longer possible for the bulk flow to be both isothermal and isoviscous. Instead, we observe in panels (b) and (d) the emergence of a quite different characteristic flow structure, with relatively warm (yellow) upper core separated from a cooler (green) lower core. The upper core is fed by hot fluid from a thermal boundary layer at the base of the cell, while the lower core is fed by cooler fluid from the lid. The average temperature in the cell is significantly lower when pressure-dependence is included, with hot fluid confined to the basal thermal boundary layer and the plume on the left boundary $x = 0$.

In Figures 2 and 3, we illustrate the effects of varying the sensitivity of the viscosity to pressure while choosing the value of ε to keep the net viscosity contrast constant. In Figure 2, we plot the temperature distributions at viscosity contrasts of 10^{20} and 10^{30} with $\mu = 0.5$ and $\mu = 1.0$. Panels (a) and (c) show the distributions for $\mu = 0.5$, which appear very similar to those for the purely temperature-dependent viscosity, although one can detect an emergent cold plume descending on the right boundary $x = 1$. With $\mu = 1.0$, this plume has developed into a relatively cold lower core near the bottom right-hand corner of the cell, while the effect of relatively warm fluid from the base is confined to an upper core region near the top left corner of the cell. Both of these features

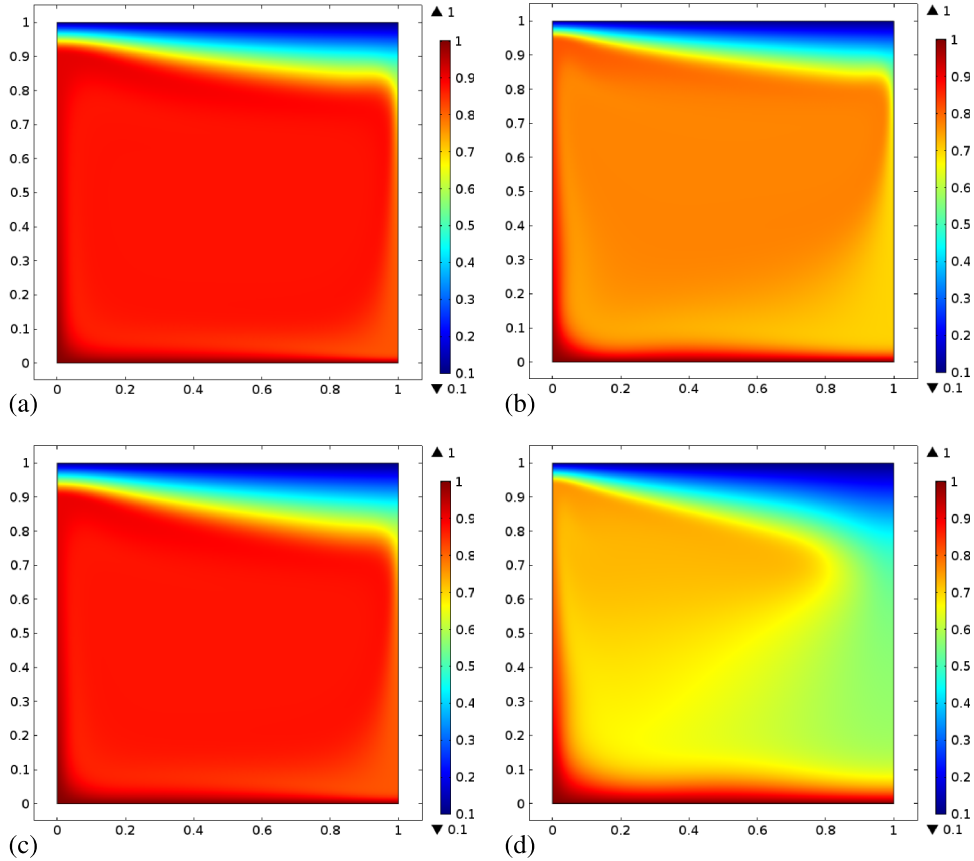


FIG. 2. Thermal distributions with different viscosity contrasts $\Delta\eta = 10^{20}$ and 10^{30} and different pressure sensitivities $\mu = 0.5$ and 1.0 , in a square cell with $\theta_0 = 0.1$ and $Ra = 10^7$. (a) $\Delta\eta = 10^{20}$, $\mu = 0.5$, $\varepsilon = 0.1846$; (b) $\Delta\eta = 10^{20}$, $\mu = 1.0$, $\varepsilon = 0.1737$; (c) $\Delta\eta = 10^{30}$, $\mu = 0.5$, $\varepsilon = 0.123$; and (d) $\Delta\eta = 10^{30}$, $\mu = 1.0$, $\varepsilon = 0.1158$.

become increasingly pronounced as the viscosity contrast increases, as seen by comparing panels (b) and (d).

The corresponding streamlines are presented in Figure 3. These are defined as contours of the streamfunction $\psi(x, z)$, defined such that

$$u = -\psi_z, \quad w = \psi_x. \quad (3.2)$$

In each case, the absence of streamlines at the top indicates the presence of a stagnant lid, but the overall convection pattern changes markedly as the pressure dependence of the viscosity becomes more important. In panel (a), where the pressure sensitivity and the net viscosity contrast are both relatively small, the flow resembles the purely temperature-dependent case, with a single large convection cell and corresponding approximately isothermal core. In contrast, panel (d) shows that with significant pressure dependence, the convective flow is concentrated in the upper core region. The values of ψ indicated on the contours indicate that the convection is much less vigorous in panel (d) than in panel (a), especially in the lower core region near the bottom right corner.

IV. LOW TEMPERATURE CUTOFF VISCOSITY

A. Motivation and validation

The computational problem becomes prohibitively stiff with further increase of the viscosity contrast. However, to obtain simulations relevant to the Earth, extremely high viscosity contrasts are necessary: the representative parameter values given in Table I suggest that $\Delta\eta$ may be 10^{50} or

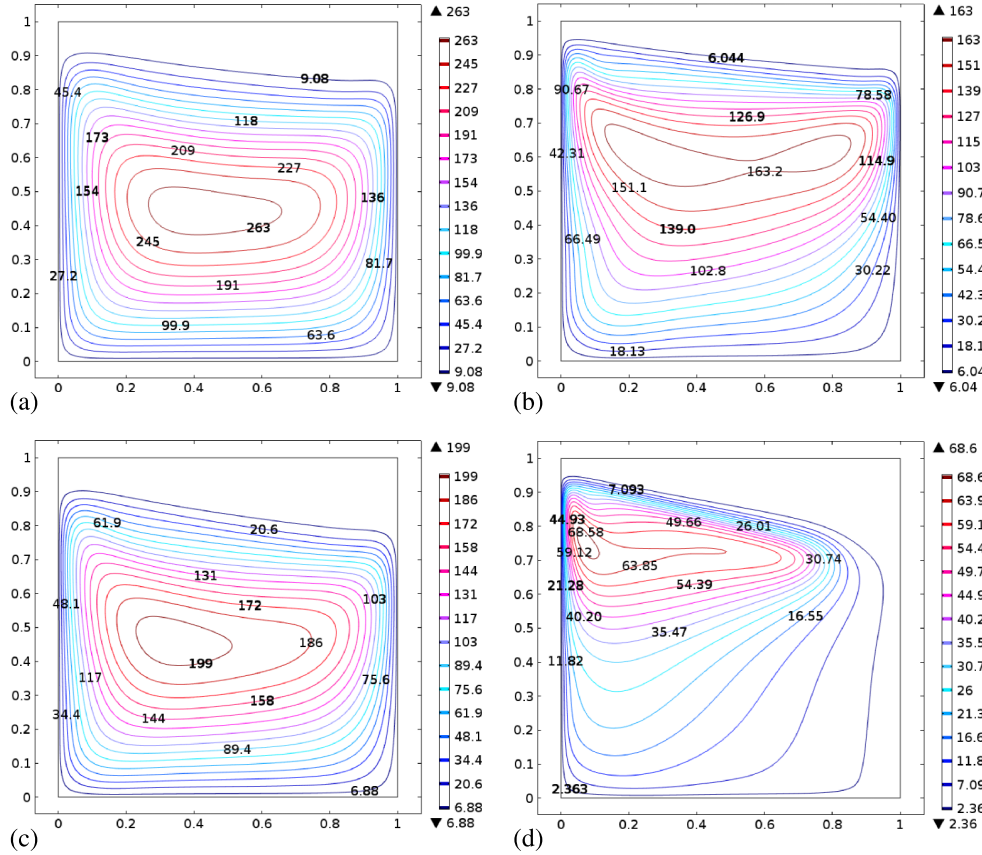


FIG. 3. Flow streamlines with different viscosity contrasts $\Delta\eta = 10^{20}$ and 10^{30} and different pressure sensitivities $\mu = 0.5$ and 1.0 , in a square cell with $\theta_0 = 0.1$ and $Ra = 10^7$. (a) $\Delta\eta = 10^{20}$, $\mu = 0.5$, $\varepsilon = 0.1846$, (b) $\Delta\eta = 10^{20}$, $\mu = 1.0$, $\varepsilon = 0.1737$, (c) $\Delta\eta = 10^{30}$, $\mu = 0.5$, $\varepsilon = 0.123$, and (d) $\Delta\eta = 10^{30}$, $\mu = 1.0$, $\varepsilon = 0.1158$.

larger. Computations have been performed previously for variable viscosity contrasts up to 10^{14} ,^{26,37} but surprisingly, this is not sufficient to establish a clear asymptotic limit for the flow. Figures 2 and 3 illustrate how, when the Rayleigh number is large and pressure dependence is included, a distinctive flow structure emerges as the viscosity contrast $\Delta\eta$ increases; however, this new regime only starts to become fully evident when $\Delta\eta$ is as large as 10^{30} . As will be demonstrated below, significant qualitative changes to the flow structure continue to occur as the viscosity contrast is increased yet further.

To overcome the difficulties associated with such extreme viscosity contrasts, we employ a trick based on the fact that, as in strongly temperature-dependent viscous convection, most of the viscosity variation occurs in a stagnant lid in which the velocity is essentially zero. We can thus calculate the sub-lid convection field accurately by cutting off the dimensionless viscosity at a sufficiently high value that the lid thickness, which essentially only depends on the interaction of the lid temperature with the underlying convecting flow, is unaffected.

We therefore propose a low temperature cutoff viscosity of the form

$$\eta = \begin{cases} \exp[M/\varepsilon] & M \leq \varepsilon \log 10^r, \\ 10^r & M > \varepsilon \log 10^r, \end{cases} \quad (4.1)$$

where

$$M = \frac{(1 + \mu)(1 - T) - \mu z}{T}, \quad (4.2)$$

and the cutoff viscosity value 10^r is to be chosen appropriately; in numerical experiments, we found that $r = 6$ gives a good compromise between accuracy and stiffness. This type of Arrhenius law

TABLE III. Nusselt number Nu and RMS velocity V_{rms} computed for convection with full-form viscosity function (2.8) and with cutoff viscosity function (4.1) at $Ra = 10^7$ and $\theta_0 = 0.1$.

$\Delta\eta$	μ	ε	Full form η		Cutoff η	
			Nu	V_{rms}	Nu	V_{rms}
10^{10}	0.5	0.369	8.040 68	999.777 5	8.044 91	999.925 5
	1.0	0.3474	9.313 42	1186.364 2	9.315 93	1186.309 4
10^{15}	0.5	0.246	6.951 03	892.717 2	6.953 66	892.744 6
	1.0	0.2316	8.172 41	956.394 8	8.173 39	956.185 65
10^{20}	0.5	0.1846	6.256 93	804.509 8	6.259 07	804.453 23
	1.0	0.174	6.896 53	614.437 14	6.896 70	614.081 43
10^{25}	0.5	0.1477	5.752 59	720.340 9	5.754 48	720.190 3
	1.0	0.139	5.496 56	317.904 07	5.496 74	317.697 97
10^{30}	0.5	0.123	5.349 14	634.447 0	5.350 85	634.186 88
	1.0	0.1158	4.921 33	273.324 3	4.923 40	273.454 68

with an imposed cutoff viscosity was applied by Huang *et al.*,³⁸ Huang and Zhong,³⁹ and King³⁶ but none of them was applied to a temperature- and pressure-dependent viscosity. We emphasise that this trick enables numerical solution of the model, without compromising the extreme viscosity variations which we seek.

To validate this proposed approximate solution approach, we compare in Table III values of the Nusselt number and the RMS velocity calculated using full viscosity function (2.8) and using cutoff viscosity function (4.1). It is evident that the agreement is uniformly excellent, with a relative error less than 0.06% throughout. Further validation is provided in Figure 4, where we show computed isothermal contours and viscosity distributions for the parameter values $\theta_0 = 0.1$, $Ra = 10^7$, $\varepsilon = 0.1158$, and $\mu = 1.0$, corresponding to a viscosity contrast $\Delta\eta = 10^{30}$. Panels (a) and (c) show the results computed using full viscosity function (2.8), while panels (b) and (d) show the corresponding results when piecewise viscosity function (4.1) is used. The qualitative and quantitative agreements are again excellent. Although the full viscosity increases 10^{30} in the lid, the cutoff value of 10^6 is already high enough for the fluid to become effectively rigid and therefore immobile.

It is again worth emphasising that, although our solution method has effectively limited the computed dimensionless viscosity to a maximum value of 10^6 , the solutions shown in Figure 4 are completely different from what would be obtained with an actual surface to base ratio of $\Delta\eta = 10^6$. At small values of ε , it is the extreme sensitivity of η to variations in T and z in the bulk flow that determines the observed structure, while the very high values of the viscosity attained in the lid are found to be unimportant. For example, it is clear in Figure 4 that the bulk fluid is far from isoviscous, and this occurs only when ε is sufficiently small, regardless of the cutoff chosen to limit the value of η in the stagnant lid.

B. Narrower convecting cells

Reassured that computations with cutoff viscosity function (4.1) accurately describe the convective flow, we are now able to compute solutions with higher viscosity contrasts corresponding to smaller values of ε . We performed a series of computations in which ε was gradually decreased while holding the other parameter values constant at $\theta_0 = 0.1$, $Ra = 10^7$, and $\mu = 1.0$. These numerical experiments revealed that convection in a square cell becomes unstable at a critical value of $\varepsilon \approx 0.1105$, corresponding to a viscosity contrast $\Delta\eta \approx 2.77 \times 10^{31}$. As ε decreases through this critical value, the convective flow breaks into a three-cell structure. The resulting temperature distribution and streamlines at $\varepsilon = 0.1105$ are shown in Figure 5, and we found that this three-cell pattern persists and is stable as ε is decreased further. This revelation leads us to hypothesise that the system copes with increasing sensitivity of the viscosity to temperature and pressure by restricting the flow to increasingly narrow convection cells.

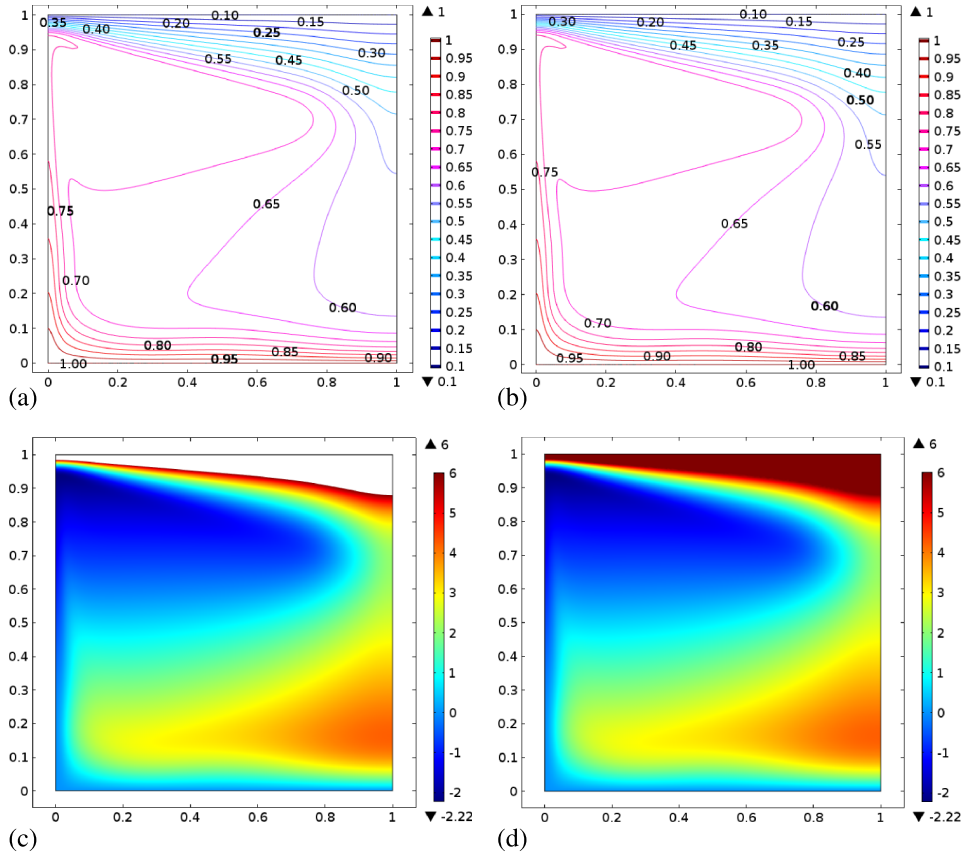


FIG. 4. Comparison of solutions from full-form viscosity model ((a) and (c)) and cutoff viscosity model ((b) and (d)) for $\theta_0 = 0.1$, $Ra = 10^7$, $\varepsilon = 0.1158$, $\mu = 1.0$. ((a) and (b)) Isothermal contours, ((c) and (d)) distribution of $\log_{10} \eta$.

Following this idea, we were able to decrease ε even further and compute solutions with even higher viscosity contrasts by simultaneously decreasing the aspect ratio of the cell. Again fixing $\theta_0 = 0.1$, $Ra = 10^7$, and $\mu = 1.0$, we found that in a 1:3 cell, stable steady solutions could be computed for ε as low as 0.085, corresponding to a viscosity contrast $\Delta\eta \approx 7.5 \times 10^{40}$. For yet smaller values of ε , stable solutions could only be found by further decreasing the cell aspect ratio. In a 1:4 cell, for example, we solved the problem for values of ε down to 0.077 (corresponding to $\Delta\eta \approx 1.3 \times 10^{45}$), and in a 1:5 cell, we obtained solutions for $\varepsilon = 0.065$ ($\Delta\eta \approx 2.8 \times 10^{53}$).

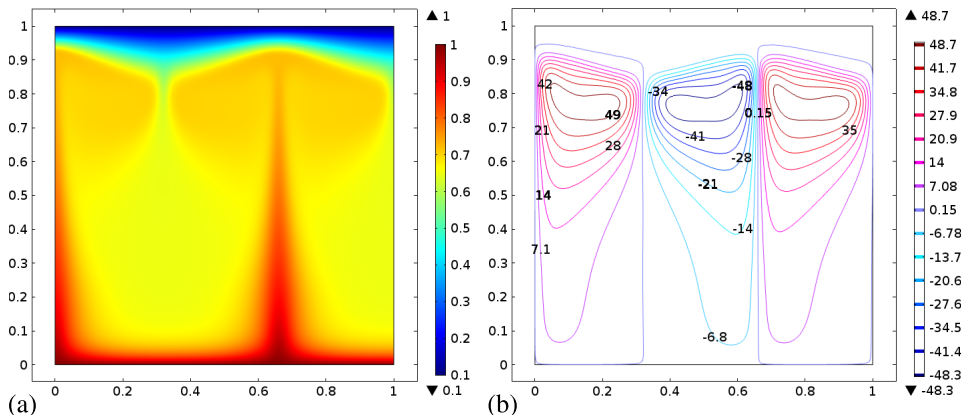


FIG. 5. Three-cell convection pattern with $\theta_0 = 0.1$, $Ra = 10^7$, $\varepsilon = 0.1105$, and $\mu = 1.0$. (a) Temperature distribution and (b) streamfunction contours.

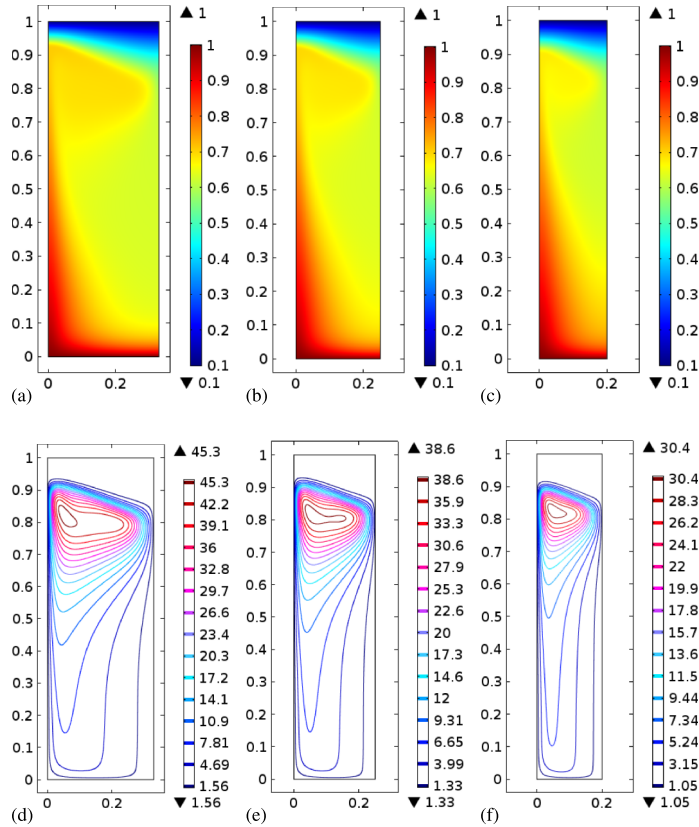


FIG. 6. Temperature distribution and streamfunction contours in cells with different aspect ratios. The parameter values are $\theta_0 = 0.1$, $Ra = 10^7$, $\mu = 1.0$, and ((a) and (d)) 1:3 cell with $\varepsilon = 0.085$; ((b) and (e)) 1:4 cell with $\varepsilon = 0.077$; ((c) and (f)) 1:5 cell with $\varepsilon = 0.065$.

The resulting temperature profiles and streamlines in cells of aspect ratios 1:3, 1:4, and 1:5 are plotted in Figure 6. Other than being compressed in the x -direction, the flow patterns in each case are strikingly similar to the 1:1 cell patterns observed above in Figures 2(d) and 3(d), for example. Below a stagnant and noticeably sloping lid, there is a rapidly circulating and relatively warm upper core, fed by a hot plume climbing the left-hand boundary of the cell. The somewhat cooler lower core is in turn fed by a descending plume from the cold lid. In all cases, the bulk fluid is neither isothermal nor isoviscous, and the flow patterns are completely different from results for purely temperature-dependent viscosity, as shown in Figures 1(a) and 1(c).

These results demonstrate that the preferred convection cell aspect ratio decreases as ε decreases, and the values found suggest that the cell width a (given unit cell height) should scale with ε . We recall that the initial breakdown of a unit aspect ratio cell occurs at $\varepsilon \approx 0.1105$, and that a three-cell pattern is then preferred, corresponding to $a = 1/3 \approx 3\varepsilon$. This scaling law is also approximately obeyed in the solutions found above with $a = 1/4$ and $a = 1/5$. We therefore hypothesise that, everything else being equal, the system prefers to adopt convection cells of width $a \propto \varepsilon$ when $\varepsilon \ll 1$, and that the constant of proportionality is around 3 when the other parameter values are $\theta_0 = 0.1$, $Ra = 10^7$, and $\mu = 1.0$.

Some numerical results obtained by varying Ra and ε while maintaining $a = 3\varepsilon$ are summarised in Figure 7, where we plot the Nusselt number Nu versus the Rayleigh number Ra for various fixed values of ε ; the other parameter values are fixed at $\theta_0 = 0.1$ and $\mu = 1.0$. At these high viscosity contrasts, Nu increases rather weakly with Ra , compared with the constant viscosity values given in Table II. At the very smallest value of $\varepsilon = 0.065$ given here, we observe that Nu reaches the value 1, implying that the flow is completely suppressed at a finite critical value of the Rayleigh number $Ra_c \approx 8.6007 \times 10^5$. To obtain further support for both this switching off of

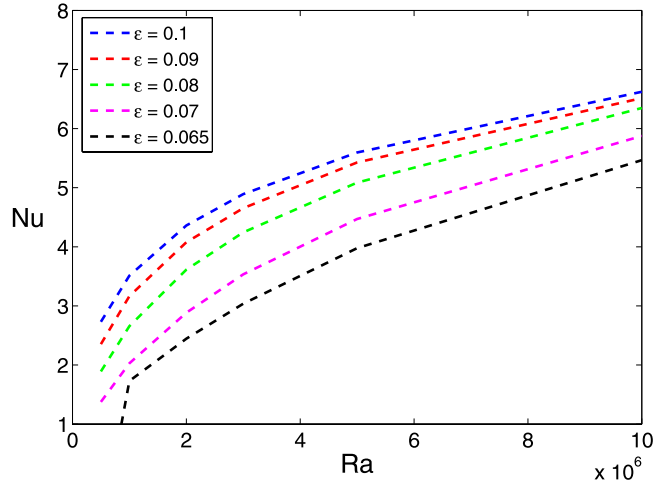


FIG. 7. Variation of Nusselt number Nu with Rayleigh number Ra at $\theta_0 = 0.1$, $\mu = 1.0$ and various fixed values of ε . In each case, the cell aspect ratio is $a = 3\varepsilon$.

the convective flow and the scaling of the cell width a with ε , we next consider a linear stability analysis.

C. Linear stability analysis

Here, we briefly summarise a linear stability analysis which predicts the critical Rayleigh number Ra_c for the onset of convection and the resulting selected wavelength. It is helpful to express governing equations (2.5) as

$$\begin{aligned} \nabla^2(\eta \nabla^2 \psi) - 4(\eta \psi_{xz})_{xz} - 2(\eta \psi_{xx})_{xx} - 2(\eta \psi_{zz})_{zz} &= Ra T_x, \\ T_t + \psi_x T_z - \psi_z T_x &= \nabla^2 T, \end{aligned} \quad (4.3)$$

where ψ is the streamfunction defined by (3.2) and η is given by Eq. (2.8). The boundary conditions are

$$\begin{aligned} \psi = \psi_{zz} = 0, \quad T = 1 \quad &\text{at } z = 0, \\ \psi = \psi_{zz} = 0, \quad T = \theta_0 \quad &\text{at } z = 1, \\ \psi = \psi_{xx} = 0, \quad T_x = 0 \quad &\text{at } x = 0, a, \end{aligned} \quad (4.4)$$

where a is the aspect ratio.

In the base state, there is no flow and a linear temperature profile, with

$$\begin{aligned} \psi &= 0, \\ T_0(z) &= 1 - (1 - \theta_0)z, \\ \eta &= \eta_0(z) = \exp\left(\frac{(1 - \theta_0 - \mu\theta_0)z}{\varepsilon(1 - (1 - \theta_0)z)}\right). \end{aligned} \quad (4.5)$$

Now, given the values of θ_0 and μ , our aim is to determine for which value of Ra this base state loses stability, in the limit as $\varepsilon \rightarrow 0$.

We observe from (4.5) that the viscosity is exponentially large unless $z = O(\varepsilon)$, and we therefore expect the initial convection to be confined to a boundary layer near $z = 0$. This motivates us to set $z = \varepsilon Z$, where $Z = O(1)$, and we then find that the base state viscosity is given to leading order by

$$\eta_0 \sim e^{\beta Z} + O(\varepsilon), \quad \text{where } \beta = 1 - (1 + \mu)\theta_0. \quad (4.6)$$

We assume that $\beta > 0$; for our chosen parameter values $\theta_0 = 0.1$ and $\mu = 1.0$, we have $\beta = 0.8$. We also anticipate that the critical wavelength at the onset of convection will be of order ε and

therefore, we linearize about base state (4.5) as follows:

$$\begin{aligned}\psi &= f(Z) \sin(kx/\varepsilon) e^{\lambda t}, \\ T &= T_0(z) + g(Z) \cos(kx/\varepsilon) e^{\lambda t},\end{aligned}\quad (4.7)$$

where λ is the linear growth rate and $k = \varepsilon\pi/a$ is the scaled wavenumber.

To lowest order in ε , the perturbation functions f and g satisfy the linearised equations

$$\begin{aligned}f'''' + 2\beta f''' + (\beta^2 - 2k^2) f'' - 2\beta k^2 f' + k^2 (\beta^2 + k^2) f &= \varepsilon^3 \text{Ra} k e^{-\beta Z} g, \\ g'' - (\varepsilon^2 \lambda + k^2) g &= -(1 - \theta_0) \varepsilon k f.\end{aligned}\quad (4.8)$$

The problem may be normalized by setting

$$Z = \frac{y}{\beta}, \quad k = \beta m, \quad \lambda = \frac{\beta^2}{\varepsilon^2} \sigma, \quad g = \frac{\beta^3}{\varepsilon^3 \text{Ra} m} h. \quad (4.9)$$

Then, Eq. (4.8) is simplified to

$$\begin{aligned}f_{yyyy} + 2f_{yy} + (1 - 2m^2) f_{yy} - 2m^2 f_y + m^2 (1 + m^2) f &= e^{-y} h, \\ h_{yy} - (\sigma + m^2) h &= -R^* m^2 f,\end{aligned}\quad (4.10)$$

where

$$R^* = \frac{(1 - \theta_0) \varepsilon^4 \text{Ra}}{\beta^4} \quad (4.11)$$

and the boundary conditions are

$$f = f_{yy} = h = 0 \quad \text{at} \quad y = 0, \quad f, h \rightarrow 0 \quad \text{as} \quad y \rightarrow \infty. \quad (4.12)$$

One can readily verify that there are sufficient degrees of freedom to satisfy the far-field conditions as $y \rightarrow \infty$.

The marginal Rayleigh number for a given wavenumber is obtained by solving the ordinary differential equations (4.10) with $\sigma = 0$, subject to boundary conditions (4.12), as an eigenvalue problem for R^* as a function of m . We then find that R^* takes its minimum $R_c^* \approx 20.8724$ when $m = m_c \approx 0.3818$. These improve the approximate values of $R_c^* \approx 20.9$ and $m_c \approx 0.395$ given by Stengel *et al.*⁴⁰

By reversing the scalings, we deduce that base state (4.5) becomes unstable when the Rayleigh number exceeds a critical value

$$\text{Ra}_c \sim \frac{R_c^*}{1 - \theta_0} \left(\frac{\beta}{\varepsilon} \right)^4. \quad (4.13)$$

As this threshold is crossed, disturbances of half-wavelength

$$a \sim \frac{\pi \varepsilon}{m \beta} \sim 8.2284 \frac{\varepsilon}{\beta} \quad (4.14)$$

are excited.

In summary, the linear stability analysis supports our hypothesis that the preferred convection cell width a should scale with ε when $\varepsilon \ll 1$. Admittedly, the constant of proportionality predicted by Eq. (4.14) with $\beta = 0.8$ is approximately 10.3 rather than the value 3 proposed in Sec. IV B. However, we should not expect the critical wavelength at onset of instability necessarily to be close to the preferred value at much larger values of the Rayleigh number. We also recall from Figure 7 that our numerical calculations predict a critical Rayleigh number $\text{Ra}_c \approx 8.6007 \times 10^5$ when $\varepsilon = 0.065$, while Eq. (4.13) predicts $\text{Ra}_c \approx 5.3 \times 10^5$. The linear stability analysis therefore produces the correct order of magnitude for Ra_c despite the fact that we had used a wavelength $a = 3\varepsilon$ rather than (4.14) in our simulations.

V. DISCUSSION

The results we have found have serious implications for the style of convection in the mantle of the Earth and other terrestrial planets. For example, we earlier estimated the viscosity contrast for the Earth's mantle is 10^{50} or more, whereas for Venus and Mars, it is around 10^{20} and 10^{50} , respectively. Extreme parameter values ensure simultaneous strong temperature and pressure dependences on the viscosity function and we have found the strong pressure dependence to have a significant effect on the dynamics. Without such extreme parameter values, we are unable to obtain a proper asymptotic structure of mantle convection for Earth and other planets. The paradigm which has emerged over the last fifty years is one of the large scale convection cells. The various phase transitions in the mantle, most notably that at 670 km, raised an early controversy on layered versus whole mantle convection, one whose resolution depends on the nature of the spinel–perovskite phase change.⁴¹ The discussion was spiced by geochemical arguments concerning different long-lived mantle reservoirs,⁴² and this led to various cartoons concerning mantle convection style.^{43,44} Nowhere has there been a suggestion that narrow convection cells might be the preferred state; the nearest comparable suggestion is that of Parsons and McKenzie⁴⁵ and Huang *et al.*,³⁸ who suggest that small scale convection in the form of transverse rolls might occur below the lithosphere.

Our thesis is that the strong pressure dependence of mantle rheology will cause, in stagnant lid convection, convection cells to be narrow and to be segregated into a vigorous upper cell with a more sluggish flow below this. This might apply on Venus, for example. What implications might there be for the Earth?

The active style of plate tectonics on the Earth, driven by the subduction of the oceanic lithosphere at plate boundaries, mitigates against the structure suggested here, at least in the upper mantle. There we would suppose that the oceanic plates drive a vigorous shallow return flow on the scale of the plates. But we suggest that the structure of the lower mantle must be similar to that shown here. The viscosity increases, and convection takes the form of narrow sluggish fingers. The details of how this might occur remain to be investigated.

VI. CONCLUSIONS

In this paper, we study numerically the Rayleigh–Bénard convection of a fluid whose viscosity depends strongly upon both temperature and pressure. Our computations are facilitated by the use of cutoff viscosity function (4.1), which allows us to access very large and previously unexplored viscosity contrasts. This approach exploits the fact that the most extreme changes in viscosity occur in the cold lid region where the flow velocity is essentially zero; without the cutoff, one ends up expending the majority of the computational effort resolving this stagnant region where very little is actually happening. By decreasing ε , we are able to study viscosity contrasts up to 10^{53} , while using the cutoff trick to limit the actual viscosity ratio in the computations to 10^6 . We find that this absolute maximum value of η achieved in the lid is unimportant: the key consequence of decreasing ε is to enhance the sensitivity of the viscosity to variations in temperature and pressure in the bulk flow.

We find that pressure dependence of the viscosity results in a new flow regime, shown for example, in Figures 2(d) and 3(d), which is completely different from the flow profile when only temperature dependence is included. Rather than a single approximately isothermal convection cell filling the whole core, we observe a warm upper core, fed by a hot plume from the base of the cell, and a quite distinct cooler lower core, fed by cold fluid from the lid. In the resulting flow profile, the fluid in the bulk is neither isothermal nor isoviscous, as suggested by Fowler.⁴⁶ It would be impossible to explore computationally the extremely high viscosity contrasts needed to observe this new flow regime without using our cutoff viscosity trick.

As ε is decreased further, a second unexpected phenomenon is observed, namely, that flow in a single square cell becomes unstable, and instead the flow breaks up into increasingly narrow convection cells. As shown in Figure 6, the flow structure appears self-similar if the aspect ratio of the cell is decreased in line with ε . This observation leads us to hypothesise that the limiting flow

structure as $\varepsilon \rightarrow 0$ consists of convection cells of width $a \propto \varepsilon$. This hypothesis is supported by a linear stability calculation; a detailed asymptotic analysis is ongoing to provide further justification of this hypothesis and a detailed description of the flow structures observed in our simulations.

ACKNOWLEDGMENTS

T. Khaleque acknowledges the award of a Felix Scholarship from the University of Oxford, U. K. and thanks her home institution University of Dhaka, Bangladesh. A. C. Fowler acknowledges the support of the Mathematics Applications Consortium for Science and Industry (www.macs.iu.ie) funded by the Science Foundation Ireland Grant No. 12/1A/1683.

- ¹ N. A. Haskell, "The viscosity of the asthenosphere," *Am. J. Sci.* **33**, 22–28 (1937).
- ² L. M. Cathles, *The Viscosity of the Earth's Mantle* (Princeton University Press, Princeton, 1975).
- ³ A. Paulson, S. Zhong, and J. Wahr, "Inference of mantle viscosity from grace and relative sea level data," *Geophys. J. Int.* **171**(2), 497–508 (2007).
- ⁴ D. L. Turcotte and E. R. Oxburgh, "Finite amplitude convective cells and continental drift," *J. Fluid Mech.* **28**, 29–42 (1967).
- ⁵ G. O. Roberts, "Fast viscous Bénard convection," *Geophys. Astrophys. Fluid Dyn.* **12**, 235–272 (1979).
- ⁶ J. Jimenez and J. A. Zufiria, "A boundary-layer analysis of Rayleigh–Bénard convection at large Rayleigh number," *J. Fluid Mech.* **178**, 53–71 (1987).
- ⁷ D. R. Moore and N. O. Weiss, "Two-dimensional Rayleigh–Bénard convection," *J. Fluid Mech.* **58**(2), 289–312 (1973).
- ⁸ G. T. Jarvis and W. R. Peltier, "Mantle convection as a boundary layer phenomenon," *Geophys. J. R. Astron. Soc.* **68**, 389–427 (1982).
- ⁹ S. H. Kirby, "Rheology of the lithosphere," *Rev. Geophys.* **21**(6), 1458–1487, doi:10.1029/RG021i006p01458 (1983).
- ¹⁰ S. Karato and P. Wu, "Rheology of the upper mantle—A synthesis," *Science* **260**(5109), 771–778 (1993).
- ¹¹ M. Armann and P. J. Tackley, "Simulating the thermochemical magmatic and tectonic evolution of venus's mantle and lithosphere: Two-dimensional models," *J. Geophys. Res.: Planets* **117**, E12003, doi:10.1029/2012je004231 (2012).
- ¹² J. Huang, A. Yang, and S. Zhong, "Constraints of the topography, gravity and volcanism on Venusian mantle dynamics and generation of plate tectonics," *Earth Planet. Sci. Lett.* **362**, 207–214 (2013).
- ¹³ G. Schubert, D. P. Turcotte, and P. Olson, *Mantle Convection in the Earth and Planets* (Cambridge University Press, Cambridge, 2001).
- ¹⁴ D. Bercovici, Y. Ricard, and M. A. Richards, "The relation between mantle dynamics and plate tectonics: A primer," in *The History and Dynamics of Global Plate Motions*, Geophysical Monograph Vol. 121, edited by M. Richards, R. Gordon, and R. van der Hilst, (A.G.U., Washington, DC, 2000), pp. 5–46.
- ¹⁵ D. Bercovici, "A simple model of plate generation from mantle flow," *Geophys. J. Int.* **114**(3), 635–650 (1993).
- ¹⁶ D. Bercovici, "The generation of plate tectonics from mantle convection," *Earth Planet. Sci. Lett.* **205**(3), 107–121 (2003).
- ¹⁷ P. J. Tackley, "Self-consistent generation of tectonic plates in three-dimensional mantle convection," *Earth Planet. Sci. Lett.* **157**(1), 9–22 (1998).
- ¹⁸ P. J. Tackley, "Self-consistent generation of tectonic plates in time-dependent, three-dimensional mantle convection simulations. 1. Pseudoplastic yielding," *Geochem., Geophys., Geosyst.* **1**(8), 1021, doi:10.1029/2000gc000036 (2000).
- ¹⁹ P. J. Tackley, "Self-consistent generation of tectonic plates in time-dependent, three-dimensional mantle convection simulations 2. Strain weakening and asthenosphere," *Geochem., Geophys., Geosyst.* **1**(8), 1026, doi:10.1029/2000gc000043 (2000).
- ²⁰ A. C. Fowler, "Boundary layer theory and subduction," *J. Geophys. Res.* **98**, 21997–22005, doi:10.1029/93JB02040 (1993).
- ²¹ A. C. Fowler and S. B. G. O'Brien, "Lithospheric failure on venus," *Proc. R. Soc. A* **459**(2039), 2663–2704 (2003).
- ²² U. R. Christensen, "Heat transport by variable viscosity convection and implications for the earth's thermal evolution," *Phys. Earth Planet. Inter.* **35**, 264–282 (1984).
- ²³ U. R. Christensen, "Convection with pressure- and temperature-dependent non-Newtonian rheology," *Geophys. J. R. Astron. Soc.* **77**, 343–384 (1984).
- ²⁴ U. R. Christensen and D. A. Yuen, "Layered convection induced by phase transitions," *J. Geophys. Res.* **90**(B12), 10291–10300, doi:10.1029/JB090iB12p10291 (1985).
- ²⁵ U. Christensen and H. Harder, "3-d convection with variable viscosity," *Geophys. J. Int.* **104**(1), 213–226 (1991).
- ²⁶ L.-N. Moresi and V. S. Solomatov, "Numerical investigation of 2D convection with extremely large viscosity variations," *Phys. Fluids* **7**(9), 2154–2162 (1995).
- ²⁷ L. Moresi and V. Solomatov, "Mantle convection with a brittle lithosphere: Thoughts on the global tectonic styles of the earth and venus," *Geophys. J. Int.* **133**(3), 669–682 (1998).
- ²⁸ C. C. Reese, V. S. Solomatov, and L.-N. Moresi, "Non-newtonian stagnant lid convection and magmatic resurfacing on venus," *Icarus* **139**(1), 67–80 (1999).
- ²⁹ C. C. Reese and V. S. Solomatov, "Mean field heat transfer scaling for non-newtonian stagnant lid convection," *J. Non-Newtonian Fluid Mech.* **107**(1), 39–49 (2002).
- ³⁰ L. Fleitout and D. A. Yuen, "Steady state, secondary convection beneath lithospheric plates with temperature-and pressure-dependent viscosity," *J. Geophys. Res.* **89**(B11), 9227–9244, doi:10.1029/JB089iB11p09227 (1984).
- ³¹ M. P. Doin, L. Fleitout, and U. Christensen, "Mantle convection and stability of depleted and undepleted continental lithosphere," *J. Geophys. Res.* **102**(B2), 2771–2787, doi:10.1029/96JB03271 (1997).
- ³² K. Stemmer, H. Harder, and U. Hansen, "A new method to simulate convection with strongly temperature-and pressure-dependent viscosity in a spherical shell: Applications to the earth's mantle," *Phys. Earth Planet. Inter.* **157**(3), 223–249 (2006).

- ³³ A. C. Fowler, *Mathematical Geoscience* (Springer, London, 2011).
- ³⁴ B. Blankenbach, F. Busse, U. Christensen, L. Cserepes, D. Gunkel, U. Hansen, H. Harder, G. Jarvis, M. Koch, G. Marquart, D. Moore, P. Olson, H. Schmeling, and T. Schnaubelt, "A benchmark comparison for mantle convection codes," *Geophys. J. Int.* **98**(1), 23–38 (1989).
- ³⁵ D. E. Koglin, Jr., S. R. Ghias, S. D. King, G. T. Jarvis, and J. P. Lowman, "Mantle convection with reversing mobile plates: A benchmark study," *Geochem., Geophys., Geosyst.* **6**, Q09003, doi:10.1029/2005GC000924 (2005).
- ³⁶ S. D. King, "On topography and geoid from 2-D stagnant lid convection calculations," *Geochem., Geophys., Geosyst.* **10**, Q03002, doi:10.1029/2008GC002250 (2009).
- ³⁷ V. S. Solomatov and L.-N. Moresi, "Stagnant lid convection on venus," *J. Geophys. Res.* **101**(E2), 4737–4753, doi:10.1029/95JE03361 (1996).
- ³⁸ J. Huang, S. Zhong, and J. van Hunen, "Controls on sublithospheric small-scale convection," *J. Geophys. Res.: Solid Earth* **108**(B8), 2405, doi:10.1029/2003JB002456 (2003).
- ³⁹ J. Huang and S. Zhong, "Sublithospheric small-scale convection and its implications for the residual topography at old ocean basins and the plate model," *J. Geophys. Res.: Solid Earth* **110**(B5), B05404, doi:10.1029/2004JD005101 (2005).
- ⁴⁰ K. C. Stengel, D. S. Oliver, and J. R. Booker, "Onset of convection in a variable-viscosity fluid," *J. Fluid Mech.* **120**, 411–431 (1982).
- ⁴¹ U. Christensen, "Effects of phase transitions on mantle convection," *Annu. Rev. Earth Planet. Sci.* **23**, 65–87 (1995).
- ⁴² P. E. van Keken and C. J. Ballentine, "Whole-mantle versus layered mantle convection and the role of a high-viscosity lower mantle in terrestrial volatile evolution," *Earth Planet. Sci. Lett.* **156**, 19–32 (1998).
- ⁴³ M. Ogawa, "Mantle convection: A review," *Fluid Dyn. Res.* **40**, 379–398 (2008).
- ⁴⁴ P. J. Tackley, "Mantle geochemical dynamics," in *Mantle Dynamics*, Treatise on Geophysics Vol. 7, edited by D. Bercovici, (Elsevier, Amsterdam, 2009), pp. 437–505.
- ⁴⁵ B. Parsons and D. McKenzie, "Mantle convection and the thermal structure of the plates," *J. Geophys. Res.* **83**(B9), 4485–4496, doi:10.1029/JB083iB09p04485 (1978).
- ⁴⁶ A. C. Fowler, "Towards a description of convection with temperature-and pressure-dependent viscosity," *Stud. Appl. Math.* **88**, 113–139 (1993).